Multimodal MRI characteristics of the glioblastoma infiltration beyond contrast enhancement

Jiun-Lin Yan, Chao Li, Natalie R. Boonzaier, Daniel M. Fountain, Timothy J. Larkin, Tomasz Matys, Anouk van der Hoorn and Stephen J. Price

Abstract: Our inability to identify the invasive margin of glioblastomas hampers attempts to achieve local control. Diffusion tensor imaging (DTI) has been implemented clinically to delineate the margin of the tumor infiltration, its derived anisotropic (q) values can extend beyond the contrast-enhanced area and correlates closely with the tumor. However, its correlation with tumor infiltration shown on multivoxel proton magnetic resonance spectroscopy[1] (MRS) and perfusion magnetic resonance imaging (MRI) should be investigated. In this study, we aimed to show tissue characteristics of the q-defined peritumoral invasion on MRS and perfusion MRI. Patients with a primary glioblastoma were included ($n = 51$). Four regions of interest were analyzed; the contrast-enhanced lesion, peritumoral abnormal q region, peritumoral normal q region, and contralateral normal-appearing white matter. MRS, including choline (Cho)/creatinine (Cr), Cho/N-acetyl-aspartate (NAA) and NAA/Cr ratios, and the relative cerebral blood volume (rCBV) were analyzed. Our results showed an increase in the Cho/NAA ($p = 0.0346$) and Cho/Cr ($p = 0.0219$) ratios in the peritumoral abnormal q region, suggestive of tumor invasion. The rCBV was marginally elevated ($p = 0.0798$). Furthermore, the size of the abnormal q regions was correlated with survival; patients with larger abnormal q regions showed better progression-free survival (median 287 *versus* 53 days, $p = 0.001$) and overall survival (median 464 *versus* 274 days, $p = 0.006$) than those with smaller peritumoral abnormal q regions of interest. These results support how the DTI q abnormal area identifies tumor activity beyond the contrast-enhanced area, especially correlating with MRS.

Keywords: diffusion tensor imaging, glioblastoma, MRI, MR spectroscopy, peritumoral area

Received: 12 October 2018; revised manuscript accepted: 25 March 2019.

Correspondence to:
Jiun-Lin Yan
Department of Neurosurgery, Chang Gung Memorial Hospital, Keelung, Taiwan
color_genie@hotmail.com

Natalie R Boonzaier
Timothy J. Larkin
Chao Li
Stephen J. Price
Cambridge Brain Tumour Imaging Laboratory, Division of Neurosurgery and Wolfson Brain Imaging Center, Department of Clinical Neuroscience, University of Cambridge, Addenbrooke's Hospital, Box 167, CB2 0QQ, Cambridge, UK

Daniel M. Fountain
School of Clinical Medicine, Cambridge University Hospitals NHS Foundation Trust, Cambridge, UK

Anouk van der Hoorn
Department of Clinical Neuroscience, University of Cambridge, Cambridge, UK
Department of Radiology (EB44), University of Groningen, Groningen, The Netherlands

Tomasz Matys
Department of Radiology, University of Cambridge, Cambridge, UK

Jiun-Lin Yan
Department of Neurosurgery, Chang Gung University College of Medicine, Taoyuan, Taiwan
Department of Neurosurery, Xiamen Chang Gung Hospital, Xiamen, Fujian, China

Introduction

Glioblastoma (GBM) is the most common primary malignant brain tumor.[1] Current treatment includes maximal safe resection, followed by radiotherapy with concomitant and adjuvant temozolomide. However, the 2-, 3-, and 5-year overall survival are only 27%, 16%, and 9.8%, respectively.[2] One of the main factors for this poor prognosis is the suboptimal local control after treatment. Up 77% of GBMs recur within 2 cm of the primary tumor,[3] and 72% of cases will recur within the radiotherapy field.[4] These treatment failures may largely be due to the inaccuracy assessment of the cancer-invasive margin; a major

limitation of current standard anatomical magnetic resonance imaging (MRI) sequences.[5] The contrast-enhanced region is the target for surgical resection, and radiotherapy will target a margin of about 2 cm around this area. However, a biopsy study has shown that tumor extends beyond the contrast-enhanced area and can even be present in areas with normal T2 signal.[6] More reliable multimodal MR techniques are thus needed to identify the GBM-invasive margin.

Different imaging modalities had been studied to show the tumor infiltration. Diffusion-weighted imaging (DWI) can detect water diffusion and

can be used to differentiate different types of edema, cellularity, and degree of the malignancy.[7] Some studies showed a high signal of DWI or apparent diffusion coefficiency (ADC) in the GBM peritumoral area.[8,9] However, it is still controversial to differentiate true tumor infiltration from the edematous brain tissue by using only DWI.[10] Diffusion tensor imaging (DTI) has been evaluated as a method that is sensitive to detect subtle white matter changes due to glioma invasion, as gliomas preferentially invade along white matter. It has been shown that DTI can identify abnormalities in the peritumoral region beyond the contrast-enhanced area which is a characteristic feature of a GBM that, for instance, is not found in brain metastases.[11] The diffusion tensor can be decomposed into isotropic component (p) and anisotropic component (q),[12] which can be used to identify whether the peritumoral white matter is infiltrated, displaced or disrupted by the GBM.[13] Complex different interactions between infiltration, displacement, and disruption can result in different p and q patterns[13,14] Most notably, the extent of resection based on DTI showed that a larger volume of resection of the DTI q values representing tumor, prolonged progression-free survival and overall survival.[15]

In addition to the diffusion magnetic resonance (MR) techniques, many different neuroimaging modalities were also been investigated to characterize the peritumoral area. Multivoxel proton MR spectroscopy (1H-MRS) derived a choline (Cho)/N-acetyl aspartate (NAA) index to represent cell turnover rate and normal neuron viability respectively. Abnormal H-MRS characteristics[1] can be seen in the peritumoral area in GBM which can be further used to differentiate GBM from the noninvasive meningioma.[16] The perfusion MR, such as dynamic susceptibility contrast MRI (DSC-MRI) can also be useful to demonstrate the peritumoral infiltration due to the angiogenesis and hyperperfusion of a GBM.[14] And the increase of the relative cerebral blood volume (rCBV) in the peritumoral nonenhanced region was found to be a poor clinical prognostic factor.[17] Other than the MRI, positron emission tomography (PET) can also be used to indicate tumor infiltration. A higher uptake in the peritumoral[11] C-methionine compared with the[18] F-fluorodeoxy-glucose had been shown to identify tumor infiltration.[18] Moreover,[11] C-methionine PET had been studied to prove more accurate planning of the radiation therapy.[19]

In this study, we aim to analyze the peritumoral tissue characteristics beyond the contrast-enhanced lesion in the abnormal and normal DTI area in correlation with 1H-MRS and DSC-MRI. It is unknown to what extent 1H-MRS and perfusion MRI corresponds to abnormal DTI-derived p and q values. Therefore, utilizing the DTI q abnormality map, peritumoral DTI-defined invasive regions of interest were compared with other peritumoral areas with normal DTI q values to provide a better understanding of the GBM local invasive environment and margin delineation.

Methods

Patient population

Patients with newly diagnosed cerebral GBM were included consecutively from our cohort between 2010 and 2014. Eligible patients include those aged over 18-years old, with a Karnofsky performance score (KPS) of more than 70, and final pathology reported as GBM. Exclusion criteria were previous cranial surgery, previous cerebral radiotherapy, or a known other primary tumor. All patients received a treatment aim of maximal surgical resection using neuronavigation (StealthStation, Medtronic, Minnesota, U.S.) and 5-aminolevulinic acid (5-ALA) fluorescence guidance. This was followed by standard radiotherapy with concomitant and adjuvant temozolomide chemotherapy.[2] Preoperative MR imaging was performed immediately preoperatively (median interval 1 day, range 0–9). Written informed written consent was obtained from every patient, and this project was approved by the local institutional review board (10/H0308/23).

MRI data acquisition

Preoperative MRI data acquisition was performed using a 3.0 T Siemens Magnetom MRI system (Siemens Healthcare, Munich, Germany) with a standard 12-channel head coil. Primary MR sequence included a volumetric 3D T1-weighted sequence with fat suppression acquired after the intravenous injection of 9 ml gadolinium (Gadovist, Bayer Schering Pharma, Berlin, Germany) (TR/TE 900/2.98 ms, inversion time 900 ms; flip angle 9°, FOV 256 × 240 mm; 176–208 slices; no slice gap; voxel size 1 mm³). T2-weighted fluid-attenuated inversion-recovery sequence and DTI acquired using a single-shot echo–planar sequence (TR/TE

8300/98 ms; flip angle 90°; FOV 192 mm²; 63 slices; no slice gap; voxel size 2 mm³) with multiple b values (0, 350, 650, 1000, 1300 and 1600 s/mm²) scanned in 12 directions. Perfusion data were acquired with a dynamic susceptibility weighted contrast-enhanced (DSC-MRI) sequence (TR/TE of 1500 ms/30; flip angle 90°; FOV 192 mm²; whole-brain coverage with a slice gap of 1.5 mm (19 slices); voxel size of $2 \times 2 \times 5$ mm). 1H-MRS was performed using chemical-shift imaging multivoxel single-slice sequence (TR/TE 2000/30–35 ms; flip angle 90°; FOV 160 mm²; voxel size $10 \times 10 \times 20$ mm).

Image processing
Preoperative diffusion, perfusion, 1H-MRS and post-contrast T1-weighted images were processed and coregistered to T2-weighted MRI using the FLIRT (FMRIB's Linear Image Registration Tool) function in the FMRIB Software Library (FSL) version 5.0.0 (available at: http://fsl.fmrib.ox.ac.uk/fsl/fslwiki/). Diffusion images were processed using FMRIB's diffusion toolbox from the FSL version 5.0.0. They were realigned to the b0 image to compensate for eddy currents and motion.[20] We further decomposed the diffusion tensor into p and q components after eigenvalues were calculated in the DTI data as previously described.[12] Perfusion data were processed using NordicICE (NordicNeuroLab AS, Bergen, Norway) and maps of rCBV were created following contrast-agent leakage correction. 1H-MRS data were processed using the LCModel.[21] The values of the Cramer–Rao lower bounds indicated by the program were used to evaluate the quality and reliability of the 1H spectra, and values with standard deviation (SD) > 20% were discarded.

Regions of interest and DTI pattern
The peritumoral abnormal q ROIs were calculated by subtracting the contrast-enhanced ROIs from the abnormal q areas in Matlab (MathWorks Inc., Natick, MA, USA). The abnormal q map was drawn manually by a neurosurgeon (JLY) using a three-dimensional (3D) slicer (http://www.slicer.org/).[22] Previous studies have shown good inter- and intrarater agreement.[10] Contrast-enhanced lesion ROIs were drawn semiautomatically by threshold selection and manual correction was made using a 3D slicer.

Four ROIs were compared for characterizing the peritumoral area outside the contrast-enhanced region (Figure 1):
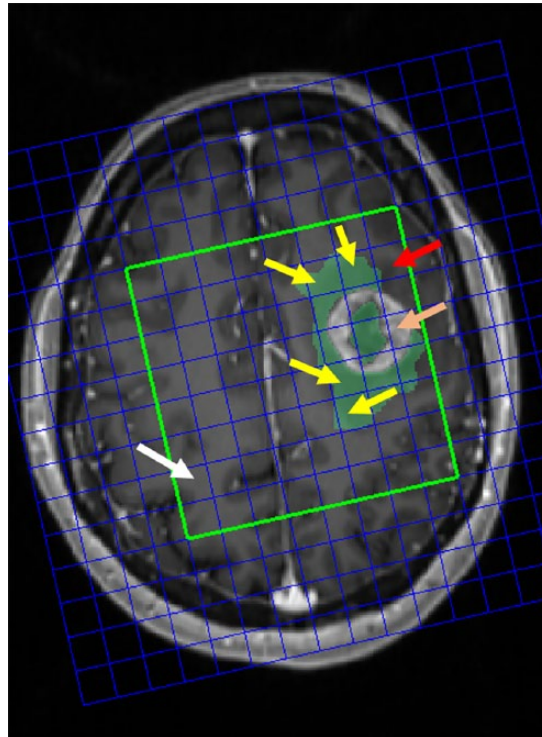

Figure 1. Illustration of the different ROIs.
Four regions of interests (ROIs) are indicated for hypothetical characteristics comparison. The red boxes indicate the peritumoral abnormal q ROIs in more than half of the MRS voxel size; the red arrow indicates the peritumoral ROIs with no q abnormality or less than half of the MRS voxel size; the orange arrow indicates the contrast-enhanced lesion; the white arrow indicates the contralateral normal-appearing white matter.
MRS, magnetic resonance spectroscopy.

(1) The peritumoral abnormal q ROIs;
(2) The peritumoral normal q ROIs;
(3) The contrast-enhanced ROIs (excluding the central necrotic part);
(4) The contralateral normal-appearing white matter (NAWM) ROIs.

Patients were classified into two groups according to the pattern of q abnormality: patients who had the q abnormal area larger than contrast-enhanced area (q > CE); and the q abnormal area equal or smaller than the contrast-enhanced areas (q ⩽ CE).

Statistics
Clinical characteristics including age, sex, percentage of the total resection of the contrast-enhanced tumor, use of gliadel wafer, isocitrate dehydrogenase-1 (IDH-1) mutation status, 6-O-methylguanine–deoxyribonucleic acid (DNA) methyltransferase
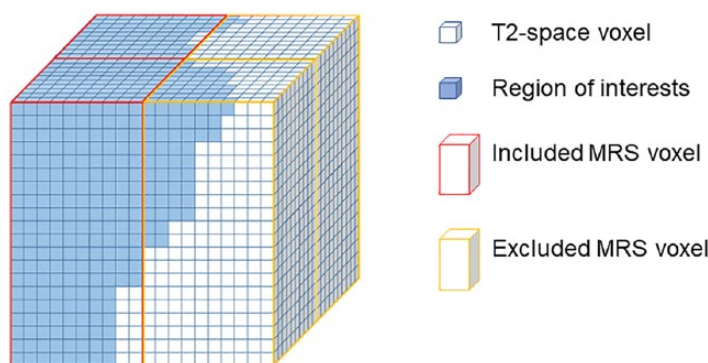
Figure 2. 3D voxel-wise method for MRS data retrieval.
This figure illustrates the 3D voxel-wise method for MRS data retrieve. White cubes represent T2-space voxel (1 mm³), and the blue cubes represent regions of interest. MRS data would be included if regions of interest occupy more than half of the MRS voxels (red outline), otherwise it would be excluded (yellow outline).
MRS, magnetic resonance spectroscopy; 3D, three dimensional.

(MGMT) methylation status, progression-free survival and overall survival were compared between the group with the q > CE and the group with the q ⩽ CE. Comparison of patients characteristics between these groups was calculated by paired *t* test for continuous data and by chi-square with Fisher's exact test for small-number categorical data. Overall survival and progression-free survival between the groups were calculated by the Kaplan–Meier method with log-rank test. All statistics were analyzed using SPSS version 22 (IBM Inc. New York, U.S.). The statistical significance was defined by two-sided *p* value < 0.05.

MR data analyses
1H-MRS tissue characteristics, including total NAA, myo-inositol (Ins), total choline (Cho) including phosphocholine (PCh) and glycerylphosphorylcholine (GPC), glutamate (Glu) and glutamine (Gln), and glutathione (GSH) were all calculated as a ratio to the total creatinine for each spectroscopy voxel. Choline/NAA ratio was also calculated. Due to a bigger size of MRS voxel ($1 \times 1 \times 2$ cm), MRS voxels were included for those ROIs occupying more than 50% of the MRS voxels. This was done by two different approaches: visual inspection; and using a 3D voxel-wise approach with an in-house program in R (R Development Core Team, 2008; Figure 2). Comparing visual inspection and 3D voxel-wise method for MRS data retrieve, no significant difference of the data value was noted between two methods (Table 1). In comparison with the visual inspection method, using 3D voxel-wise method had two more sets of missing data in Cho/Cr, three

more sets in Ins/Cr, one more set in Glu + Gln/Cr and one set fewer in Cho/NAA. On the other hand, one more missing set was found in the visual inspection method than the 3D voxel-wise method. Although not significantly different, the 3D voxel-wise method had more objectivity for MRS data retrieval and eliminated potential visual bias. We therefore use this method in our paper.

MRS data and rCBV between different ROI groups were compared by using one-way analysis of variance test and paired *t* test was used to compare imaging data between the peritumoral abnormal q ROIs and those outside abnormal q ROIs. This was also done using SPSS version 22 (IBM Inc.) with statistical significance defined by a two-sided *p* value < 0.05.

Results
We included 51 patients (mean age 58.4 years, range 36.7–73.8) in this study. There were 12 females and 39 males. The complete resection based on contrast-enhanced T1-weighted MRI was achieved in 76% of the patients. IDH-1 mutation status was obtained in 32 patients, and 3 (9%) were mutated. MGMT promoter methylation status was available in 32 patients with 16 (50%) patients methylated. The overall survival was 484 days ± 312 days (median ± SD), and the progression-free survival was 121 ± 130 days. All ROIs (peritumoral abnormal q ROIs; peritumoral normal q ROIs; contrast-enhanced ROIs and contralateral NAWM ROIs) were extracted from all patients. Also, all spectroscopy spectra could be extracted for all patients.

Table 1. Comparison of different methods for MRS data retrieval.

	3D voxel-wise approach		Visual inspection		*p* value
	Value	**Number of included voxels**	**Value**	**Number of included voxels**	
Cho/Cr	0.486 ± 0.042	25	0.442 ± 0.021	27	0.3733
NAA/Cr	0.913 ± 0.059	25	0.946 ± 0.061	25	0.6995
Cho/NAA	0.731 ± 0.131	25	0.639 ± 0.149	24	0.6431
Ins/Cr	1.373 ± 0.121	23	1.207 ± 0.064	26	0.2164
Glu + Gln /Cr	1.842 ± 0.237	19	1.772 ± 0.138	20	0.3951

Cho, choline; Cr, creatinine; NAA, N-acetyl-aspartate; Ins, myo-inositol; Glu, glutamate; Gln, glutamine, 3D, three dimensional.
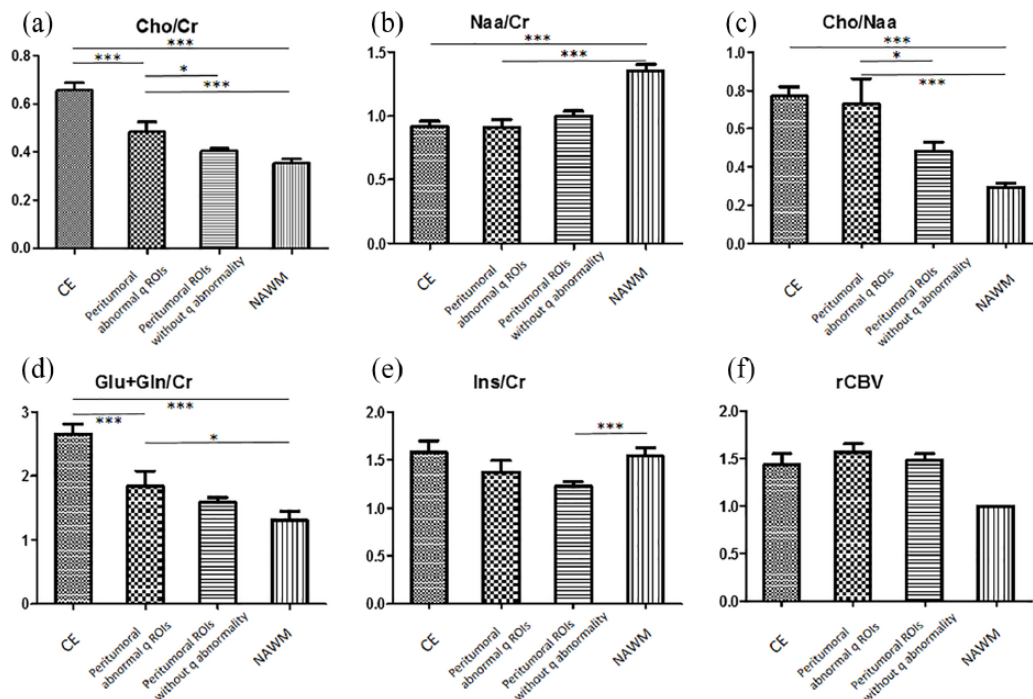
Figure 3. MRS and perfusion characteristics between different ROIs.
The MRS data of different chemical compounds (a–e) and rCBV (f) between different regions of interest (ROIs) are shown. The contrast-enhanced ROI (CE), peritumoral abnormal q ROIs and the peritumoral ROIs without q abnormality, and the control contralateral normal-appearing white matter (NAWM) are demonstrated.
*$p < 0.05$.
**$p < 0.01$.
***$p < 0.001$.

1H-MRS tissue characteristics using the 3D voxel-wise method

Using the 3D voxel-wise approach for 1H-MRS data retrieve, Cho/Cr were different in all four ROIs [$p < 0.0001$, Figure 3(a)], highest in the contrast-enhanced ROIs, followed by peritumoral abnormal q ROIs, peritumoral normal q ROIs, and the control NAWM. Subgroup analysis
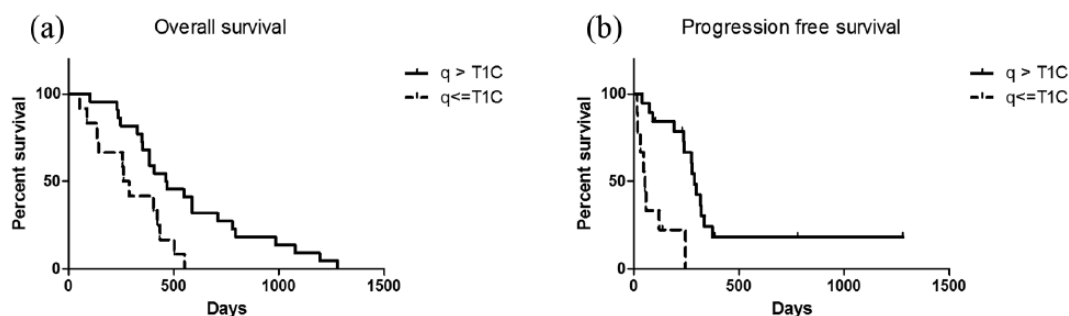
Figure 4. Survival difference between different q abnormality patterns.
Figure 4 shows the different overall survival between different q abnormality patterns. For patients with q abnormal ROIs larger than contrast-enhanced area, log-rank test showed a longer overall survival than patients with smaller q abnormal ROIs [4(a), $p = 0.0055$]. Furthermore, progression-free survival was also longer in the larger q abnormal ROIs group [4(b), $p = 0.0013$].

showed higher Cho/Cr in the peritumoral q abnormality area than the peritumoral normal q area ($p = 0.0219$). Total NAA/Cr showed an increase in the contrast-enhanced ROIs [$p < 0.0001$, Figure 3(b)], but no significant difference between peritumoral q abnormal ROIs and normal q ROIs ($p = 0.3532$). Significant elevation of Cho/NAA ratio was noted in the contrast-enhanced ROIs [$p < 0.0001$, Figure 3(c)]. In peritumoral q abnormal ROIs, an increase in the Cho/NAA ratio was seen compared with the normal q ROIs ($p = 0.0346$) and control NAWM ($p = 0.0021$). The Glu/Cr was found to be higher over the contrast-enhanced ROIs and peritumoral q abnormal ROIs than the control NAWM [$p < 0.0001$ and $p = 0.0158$, respectively; Figure 3(d)]. Glu/Cr of the abnormal q ROIs was not statistically significantly different from the normal q ROIs ($p = 0.6981$) and control ($p = 0.0682$). However, there was a significant decrease in Ins/Cr in the peritumoral abnormal q ROIs, compared with the contrast-enhanced ROIs and control NAWM [$p < 0.0001$ and $p = 0.0011$, respectively; Figure 3(e)].

rCBVs were higher in contrast-enhanced ROIs and all peritumoral areas than the control NAWM ($p < 0.0001$). Subgroup analysis showed marginal increase of rCBV in peritumoral q abnormal ROIs compared with the peritumoral normal q ROIs [$p = 0.0798$, Figure 3(f)].

Clinical outcome of different q abnormality patterns
A total of 28 out of 51 patients had the q abnormality area greater than the contrast-enhanced area for at least ½ of the MRS voxel, while 23 out

of 51 patients had q abnormality area equally or smaller than the enhanced area. The overall survival was significantly longer than those with a larger q abnormality area [median: 464 *versus* 274 days, $p = 0.0055$; Figure 4(a)]. And the progression-free survival is also longer in this larger q abnormal ROIs group (median: 287 *versus* 53 days, $p = 0.0013$). A bias from other patients characteristics is unlikely as there were no statistical difference in age, gender, total resection of the contrast-enhanced lesion, use of gliadel wafer, MGMT methylation status and IDH-1 mutation status between two groups of patients (Table 2).

Discussion
In this study, the abnormal peritumoral q area indicative of tumor infiltration beyond the contrast-enhanced area corresponded to tumor infiltration on 1H-MRS with an increase in Cho/NAA and Cho/Cr. Furthermore, a higher rCBV was also suggested. This provides support for the delineation of the tumor infiltration margin with DTI. The is of particular relevance, as abnormal DTI q ROIs demonstrated an impact on survival. It is clear that GBM cells can extend beyond contrast-enhanced lesions, as previously, researchers showed tumor infiltration of the peritumoral region outside the contrast enhancement on biopsy studies in up to one third of patients.[23] However, conventional structural MRI sequences fail to detect this invasive margin. Many studies have attempted to use multimodal MRI of the peritumoral areas to differentiate GBM from less invasive metastatic brain tumors or benign brain tumors.[14] DTI is promising for showing peritumoral infiltration. Min and colleagues showed a significant higher

Table 2. Clinical characteristics in patients with a different q abnormality pattern.

	q ≤ T1C	q > T1C	*p* value
n	23	28	
Age, years (mean ± SD)	60.09 ± 2.312	57.40 ± 2.061	0.490
Sex (M/F, %)	50/50	84/17	0.061
Complete resection CE (% of patients)	75	75	n.s.
Gliadel use (%)	56.25	70.8	0.486
IDH-1 mutation (*n*)	1	3	0.609
MGMT methylation (*n*)	9	11	n.s.
Progression-free survival (days)	53	287	0.001
Overall survival (days)	274	464	0.006

Patients with q abnormality areas smaller or equal to contrast-enhanced areas (q ≤ T1C) are compared with patients with q abnormality areas larger than the contrast-enhanced areas for more than half of MRS voxel size (q > T1C).
CE, contrast enhanced; IDH-1, isocitrate dehydrogenase-1; MGMT, O6-methylguanine-deoxyribonucleic acid methyltransferase; MRS, magnetic resonance spectroscopy; n.s., not significant; SD, standard deviation; T1C, contrast-enhanced areas.

regression coefficiency of radial diffusivity to axial diffusivity and a lower fractional anisotropy (FA);[24] and Wang and colleagues also showed a decrease in the q component of DTI in the peritumoral area. Furthermore, our previous biopsy studies also showed that abnormal DTI, especially in the q area, represents tumor-cell infiltration.[13] Therefore, DTI can better define the GBM-invasive margin.[14] Although other non-q DTI is not demonstrated by all. Tsougos and colleagues showed inconsistent results of DTI in the peritumoral areas, with no difference in the ADC or FA between the peritumoral area and control area.[25]

It this study, we showed that tumor infiltration of the abnormal q area corresponds with tumor infiltration detection on 1H-MRS. Our results showed an increase in cell turnover rate (increase in Cho/Cr) in the peritumoral region in the abnormal q ROIs, which was also significantly higher compared with the peritumoral normal q ROIs. Although NAA/Cr showed no difference between abnormal q and normal q ROIs, NAA/Cr in all peritumoral ROIs were lower than the contralateral control which is compatible with other studies. Tsougos and colleagues had shown an increase in Cho/Cr, rCBV and a decrease in NAA/Cr were found in the peritumoral areas of GBM compared with metastatic tumors.[25] Other studies showed an increase in Cho/Cr, Cr/NAA, and Ins/Cr.[16] In our

results, an increase of Glu/Cr in both the contrast-enhanced ROIs and in the peritumoral abnormal q ROIs compared with the contralateral control NAWM indicates tumor activity and the Glu is known to play an important role in tumor invasion.[26] Therefore, this showed an increase in invasive potential from these peritumoral q abnormal ROIs. Next, our results showed a decreased level of Ins/Cr in the peritumoral ROIs especially in the q normal area. Ins is known as a cerebral osmolyte and astrocyte marker that can be seen in various intracranial pathology.[27] Therefore, a decrease in Ins/Cr may be due to peritumoral brain edema.[26] Besides, compared with the contralateral control, our results did not show a decrease of Ins/Cr in the contrast-enhanced area. The increase of Ins/Cr can be due to astrocytosis or myelin destruction. But the change of the Ins/Cr level is variable: Castillo and colleagues showed an increase of Ins/Cr in low-grade glioma and a decrease in GBM.[28] This result may be due to a possible elevation of the Ins/Cr in the contralateral NAWM that Kellenberg and colleagues had described, where possible tumor infiltration in the contralateral cerebral hemisphere of the untreated GBM patients was associated with an increase of Ins.

Our DSC-MRI showed marginal higher rCBV in the peritumoral abnormal q ROIs than in the normal q ROIs ($p = 0.0798$). This is supported by

previous studies showing increased peritumoral rCBV in GBM (REF). An increase of rCBV results in increased tumor density followed by hypoxia then angiogenesis, which is correlated with cellular proliferation in high-grade glioma.[29] Other groups have shown that the site of increased rCBV may potentially also predict sites of tumor progression.[30]

Lastly, our study has shown that different patterns of abnormal q ROIs impact clinical outcome. We have shown that there is a better overall survival and progression-free survival in those with larger abnormal q ROIs than contrast-enhanced areas. This was independent of age, resection type, IDH-1 mutation status and MGMT methylation status between two groups. And all patients in our cohort were KPS > 70 and received the same treatment protocol including 5-ALA-guided surgical resection followed by postoperative temozolomide chemoradiotherapy and adjuvant temozolomide therapy. Our previous studies showed DTI abnormality patterns can be classified into localized, minimal and diffused types and are associated with prognosis.[31] The classification was based on the relationship of p and q abnormal areas but not with the contrast-enhanced area. Different invasion patterns thus might result in different prognoses. Furthermore, the abnormal q ROIs representing tumor-cell infiltration showed a higher Cho/Cr level, which represents a higher cell turnover rate. Although a better survival in patients with more abnormal q indicating tumor might seem contra-intuitive, higher Cho in the abnormal q region is hypothesized to facilitate increased chemoradiosensitivity, which may explain the better survival in these patients. However, a guided biopsy study is needed in future to correlate the MRS, biologic characteristics, and this clinical presentation. And our better survival in relation to a higher Cho is, however, not widely supported, as a small study with 14 patients showed that lower baseline NAA/Cr and higher Cho/Cr in the peritumoral nonenhanced region were associated with poor outcome.[32]

A common limitation in 1H-MRS studies is a visual selection of the MRS voxels. Most studies use visual inspection by an experienced expert to select the MRS voxel from the overlaying ROIs. However, as the MRS voxel is usually larger than other MRI sequences, and the shape of the GBM often grows irregularly. We used two different methods to select ROIs in MRS voxel. Next, to visually inspect, we performed a 3D voxel-wise approach with which the MRS data were automatically retrieved according to the different ROIs. This may minimize possible error in visual inspection. By using this method, we found more missing data that showed this automatic selection had a higher standard on the MRS voxel quality control. Although there was no statistical difference between the metabolite values of the two methods, this still provides a more objective method for MRS data retrieval and eliminates possible visual bias.

Another limitation of our study is that 5-ALA is used during surgery. This might influence the survival of the patients as it can potentially influence the extent of the resection of the peritumoral nonenhanced area.[33] As 5-ALA is used in all patients, a potential bias in survival is expected to equally influence all patients.

In conclusion, the peritumoral invasive margin can be identified by using DTI q. In ROIs of peritumoral abnormal q area, there was higher Cho/NAA and Cho/Cr which indicates tumor activity. Also, rCBV was marginally elevated in line with tumor infiltration. In addition, different patterns of the peritumoral abnormal q may have clinical implication as a larger abnormal q than contrast-enhanced lesion showed a better progression-free survival and overall survival. Our results demonstrate the relevance of the peritumoral area and indicate its potential target for therapeutic interventional studies.

Conflict of interest statement
The authors declare that there is no conflict of interest.

Reference
1. Ostrom QT, Gittleman H, Liao P, *et al.* CBTRUS statistical report: primary brain and central nervous system tumors diagnosed in the

United States in 2007-2011. *Neuro Oncol* 2014; 16(Suppl. 4): iv1–63.

2. Stupp R, Hegi M, Mason WP, *et al.* Effects of radiotherapy with concomitant and adjuvant temozolomide versus radiotherapy alone on survival in glioblastoma in a randomised phase III study: 5-year analysis of the EORTC-NCIC trial. *Lancet Oncol* 2009; 10: 459–466.

3. Sherriff J, Tamangani J, Senthil L, *et al.* Patterns of relapse in glioblastoma multiforme following concomitant chemoradiotherapy with temozolomide. *Br J Radiol* 2013; 86: 20120414.

4. Brandes AA, Tosoni A, Franceschi E, *et al.* Recurrence pattern after temozolomide concomitant with and adjuvant to radiotherapy in newly diagnosed patients with glioblastoma: correlation with MGMT promoter methylation status. *J Clin Oncol* 2009; 27: 1275–1279.

5. Price SJ and Waldman AD. Advances in imaging brain cancer. *Emerg Concepts Neurooncol.* 2013; 119–140.

6. Price SJ and Gillard JH. Imaging biomarkers of brain tumour margin and tumour invasion. *Br J Radiol* 2011; 84(Spec No 2): S159–S167.

7. Kalpathy-Cramer J, Gerstner ER, Emblem KE, *et al.* Advanced magnetic resonance imaging of the physical processes in human glioblastoma. *Cancer Res* 2014; 74: 4622–4637.

8. Kolakshyapati M, Adhikari RB, Karlowee V, *et al.* Nonenhancing peritumoral hyperintense lesion on diffusion-weighted imaging in glioblastoma: a novel diagnostic and specific prognostic indicator. *J Neurosurg* 2018; 128: 667–678.

9. Deng Z, Yan Y, Zhong D, *et al.* Quantitative analysis of glioma cell invasion by diffusion tensor imaging. *J Clin Neurosci* 2010; 17: 1530–1536.

10. Pauleit D, Langen KJ, Floeth F, *et al.* Can the apparent diffusion coefficient be used as a noninvasive parameter to distinguish tumor tissue from peritumoral tissue in cerebral gliomas? *J Magn Reson Imaging* 2004; 20: 758–764.

11. Jiang R, Du FZ, He C, *et al.* The value of diffusion tensor imaging in differentiating high-grade gliomas from brain metastases: a systematic review and meta-analysis. *PLoS One* 2014; 9: e112550.

12. Pena A, Green HA, Carpenter TA, *et al.* Enhanced visualization and quantification of magnetic resonance diffusion tensor imaging using the p:q tensor decomposition. *Br J Radiol* 2006; 79: 101–109.

13. Price SJ, Jena R, Burnet NG, *et al.* Improved delineation of glioma margins and regions of infiltration with the use of diffusion tensor imaging: an image-guided biopsy study. *AJNR Am J Neuroradiol* 2006; 27: 1969–1974.

14. Price SJ, Young AM, Scotton WJ, *et al.* Multimodal MRI can identify perfusion and metabolic changes in the invasive margin of glioblastomas. *J Magn Reson Imaging* 2016; 43: 487–494.

15. Yan JL, Van der Hoorn A, Larkin TJ, *et al.* Extent of resection of peritumoral diffusion tensor imaging-detected abnormality as a predictor of survival in adult glioblastoma patients. *J Neurosurg* 2017; 126: 234–241.

16. Wijnen JP, Idema AJ, Stawicki M, *et al.* Quantitative short echo time 1H MRSI of the peripheral edematous region of human brain tumors in the differentiation between glioblastoma, metastasis, and meningioma. *J Magn Reson Imaging* 2012; 36: 1072–1082.

17. Jain R, Poisson LM, Gutman D, *et al.* Outcome prediction in patients with glioblastoma by using imaging, clinical, and genomic biomarkers: focus on the nonenhancing component of the tumor. *Radiology* 2014; 272: 484–493.

18. Kinoshita M, Goto T, Arita H, *et al.* Imaging (1)(8)F-fluorodeoxy glucose/(1)(1)C-methionine uptake decoupling for identification of tumor cell infiltration in peritumoral brain edema. *J Neurooncol* 2012; 106: 417–425.

19. Grosu AL, Weber WA, Riedel E, *et al.* L-(methyl-11C) methionine positron emission tomography for target delineation in resected high-grade gliomas before radiotherapy. *Int J Radiat Oncol Biol Phys* 2005; 63: 64–74.

20. Jenkinson M and Smith S. A global optimisation method for robust affine registration of brain images. *Med Image Anal* 2001; 5: 143–156.

21. Provencher SW. Estimation of metabolite concentrations from localized in vivo proton NMR spectra. *Magn Reson Med* 1993; 30: 672–679.

22. Fedorov A, Beichel R, Kalpathy-Cramer J, *et al.* 3D Slicer as an image computing platform for the Quantitative Imaging Network. *Magn Reson Imaging* 2012; 30: 1323–1341.

23. Lemee JM, Clavreul A, Aubry M, *et al.* Characterizing the peritumoral brain zone in glioblastoma: a multidisciplinary analysis. *J Neurooncol* 2015; 122: 53–61.

24. Min ZG, Niu C, Rana N, *et al.* Differentiation of pure vasogenic edema and tumor-infiltrated edema in patients with peritumoral edema by analyzing the relationship of axial and radial

diffusivities on 3.0T MRI. *Clin Neurol Neurosurg* 2013; 115: 1366–1370.

25. Tsougos I, Svolos P, Kousi E, *et al*. Differentiation of glioblastoma multiforme from metastatic brain tumor using proton magnetic resonance spectroscopy, diffusion and perfusion metrics at 3 T. *Cancer Imaging* 2012; 12: 423–436.

26. Cordoba J, Gottstein J and Blei AT. Glutamine, myo-inositol, and organic brain osmolytes after portocaval anastomosis in the rat: implications for ammonia-induced brain edema. *Hepatology* 1996; 24: 919–923.

27. Tran T, Ross B and Lin A. Magnetic resonance spectroscopy in neurological diagnosis. *Neurol Clin* 2009; 27: 21–60, xiii.

28. Castillo M, Smith JK and Kwock L. Correlation of myo-inositol levels and grading of cerebral astrocytomas. *AJNR Am J Neuroradiol* 2000; 21: 1645–1649.

29. Price SJ, Green HA, Dean AF, *et al*. Correlation of MR relative cerebral blood volume measurements with cellular density and proliferation in high-grade gliomas: an image-guided biopsy study. *AJNR Am J Neuroradiol* 2011; 32: 501–506.

30. Blasel S, Franz K, Ackermann H, *et al*. Stripe-like increase of rCBV beyond the visible border of glioblastomas: site of tumor infiltration growing after neurosurgery. *J Neurooncol* 2011; 103: 575–584.

31. Mohsen LA, Shi V, Jena R, *et al*. Diffusion tensor invasive phenotypes can predict progression-free survival in glioblastomas. *Br J Neurosurg* 2013; 27: 436–441.

32. Balmaceda C, Critchell D, Mao X, *et al*. Multisection 1H magnetic resonance spectroscopic imaging assessment of glioma response to chemotherapy. *J Neurooncoly* 2006; 76: 185–191.

33. Schucht P, Knittel S, Slotboom J, *et al*. 5-ALA complete resections go beyond MR contrast enhancement: shift corrected volumetric analysis of the extent of resection in surgery for glioblastoma. *Acta Neurochir (Wien)* 2014; 156: 305–312; discussion 312.